Evolution of a Suite of Computational Modeling Tools for Mobile Telephone Dosimetry Studies at the University of Bradford, U.K.

Peter S. Excell and John A. Vaul
University of Bradford, UK

Abstract

The evolution of a set of software and skills for the computational simulation of the interaction of mobile telephones with the human body is reviewed. These have been developed and applied in the authors' research group over the past decade. The work has aimed at maximization of realism in the representation of the body components and the telephone through use of MRI images, use of resolutions down to 1mm, incorporation of a hand into the model, development of a rotation algorithm for the telephone, development of techniques for modeling helical antennas, and development of hybrid techniques to allow the Method of Moments to be used to model the telephone, combined with finite difference methods for the human tissues. Generic experience and specimen results are presented. It is argued that the policy of pursuing realism in the simulation, beyond the level that is sufficient on physical grounds, is essential to convince the non-specialist public of the trustworthiness of the work.

Keywords: Radiofrequency dosimetry; Specific absorption rate; Finite difference time domain method; Modeling verisimilitude; Human head; Human hand; Magnetic resonance image.

1. Introduction

This paper describes the evolution of software and skills for the computational simulation of the interaction of mobile telephones with the human body, developed over a period of ten years within the authors' research group. A major mission of this group throughout this period has been to maximize the realism of the simulation, within the boundaries of what has been feasible with contemporary computer technology. To this end, the following innovations were developed for, or introduced into, the work as soon as they were feasible:

1. Use of three-dimensional magnetic resonance image of human head
2. Semi-automatic segmentation and classification software to convert the head image to a form classified by microwave properties
3. Targeting of 1mm resolution in voxel models of human head
4. Use of parallel computers to handle high resolution models
5. Incorporation of a simplified human hand into the model, but with the addition of a protruding thumb
6. Development of a rotation algorithm for the mobile telephone, including compensation for the 'staircasing' effect of the finite difference grid on a wire that is not parallel to one of the principal axes
7. Recognition that the monopole antenna has declined in significance and that new techniques were needed for modeling the more popular normal-mode helical antennas
8. Development of highly-detailed models of helical antennas, including non-uniform current distributions and transverse currents in the wires due to winding capacitance
9. Development of hybrid computational techniques to allow the Method of Moments to be used to model the telephone, combined with finite difference methods for the human tissues
10. Development of a fully articulated simulation of the human hand, to allow realistic grasping of telephones of diminishing size.

The work was driven by national and international projects intended to refine and stabilize computational and physical techniques for determination of the specific absorption rate (SAR) in the body due to mobile telephones. The chief among these projects were IBREHT (Interaction of the Body with Radiated Emissions from Handheld Transceivers), a UK national project funded jointly by the UK government and nine industrial partners [1], PEPSE (Parallel Electromagnetic Programming Support Environment), a project funded by the European Union, with five partners [2], and CEPHOS (Cellular Phone Standard), another European Union project, having 15 partners spread across the Continent [3,4].

2. Early Results (IBREHT Project)

When the IBREHT project was commenced in 1991, the initial thinking was that a hybrid computational technique would be desirable, to enable coupling of a Moment-Method model of the antenna to a finite-difference model of the head. The well-known program GEMACS [5] was evaluated as a candidate, since it includes hybridization of the Method of Moments, a finite-difference frequency-domain (FDFD) formulation, and the GTD method. Unfortunately, at that time, the FDFD formulation was intended for, and was only really suitable for, cavities of moderate electrical size penetrating metallic structures (e.g. aircraft cockpits). The possibility of re-working the software to allow finite difference modeling of the human head was considered, but it appeared that the size of the

computational task would be beyond the capability of realistic contemporary computers. Thus, as happened in many other groups around the same time, it was concluded that the finite difference time domain method, by itself, appeared to offer the optimum solution. Later, the idea of using a hybrid approach was re-activated and the pioneering work of the authors of GEMACS in this area deserves appropriate recognition.

The FDTD software chosen was an updated version of THREDE [6], using the Fang-Mei [7] 'Superabsorption' boundary treatment and incorporating a thin wire model [8], but with modifications to allow a large region of inhomogeneous dielectric to be treated, with electrical properties specified on a per-cell basis. Extensive validation studies were undertaken, comparing the results of the program with those from Mie-series modeling of dielectric spheres and direct measurements of the fields.

Computed values of SAR, at 900 and 1800 MHz, using the Mie-Series and FDTD techniques were compared. The spheres were irradiated by an incident plane wave (1 V/m amplitude) with vector propagation constant parallel to, and polarization normal to, the equatorial plane. The resolution for the FDTD models was 2.5 mm in all cases. The SAR was formed by using three cartesian components of electric field at the same corner of each cell, for reasons of computational simplicity, although recent work [9] suggests that using all twelve electric fields of the FDTD cell to obtain the total electric field corresponding to each voxel leads to more accurate evaluation of 1g mass-averaged SAR values. Fig. 1 illustrates the SAR values along a line in the centre of the equatorial plane and parallel to the vector propagation constant. The agreement between the two methods is seen to be excellent, thus justifying the choice of method and absorbing boundary condition (ABC).

The sphere represented in fig. 1 had an outside diameter of 20cm, with a core of brain surrounded by four 5mm layers simulating cerebro-spinal fluid, dura, bone and skin. The electrical properties were as shown in Table 1.

Table 1: Benchmark Test Sphere Properties [10,11*]

Layer	Radius m	ε_r		σ (S/m)	
		900 MHz	1800 MHz	900 MHz	1800 MHz
Brain (core)	0.085	50	43	1.00	1.93
CSF	0.090	84	84	0.90	1.20
Dura*	0.0925	48	48	0.90	1.20
Bone*	0.0975	8	8	0.11	0.15
Skin*	0.10	35	32	0.60	0.57

2.1 Head Image

For a realistic representation of the human head, a magnetic-resonance image (MRI) was acquired from the public-domain visualization database at the University of North Carolina. This had a spatial resolution of approximately 1mm and was a single-band and gray-scale image with 8-bit amplitude resolution. This could not be converted directly to a 3-dimensional map of the bulk tissues with individually homogenized microwave properties, but a semi automatic procedure (supervised classification) was developed to enable it to be converted to such a map, 13 distinctive bulk tissues being represented. This image has been extensively used as a standard test piece, having been licensed to several other laboratories (fig. 2) [12].

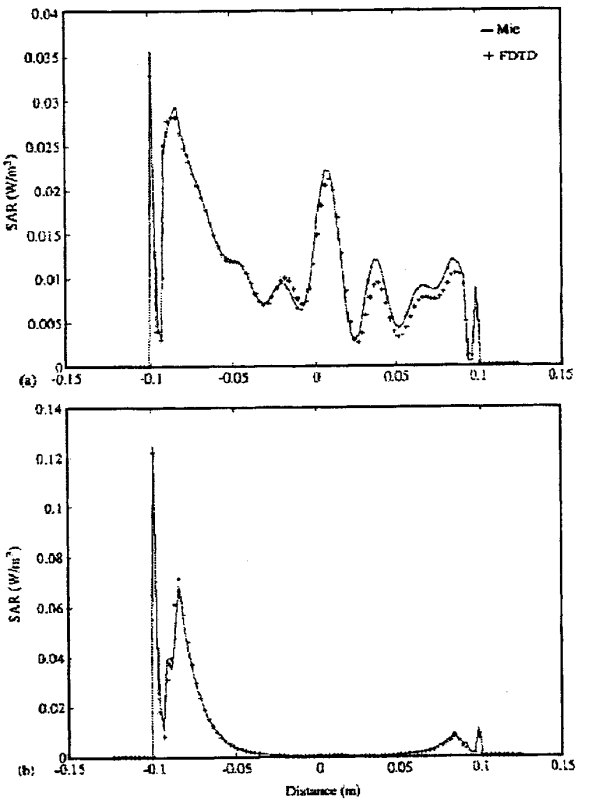

Fig. 1. Overlaid comparison of Mie-series and FDTD simulation of SAR within sphere simulating human head: (a) 900 MHz; (b) 1.8 GHz.

2.2 Mobile Phone Representation

The telephone was represented by a rectangular chassis, surmounted by a monopole antenna, but following earlier studies by Luebbers [13] it was encased in a layer of non-conducting dielectric (plastic case). This was clearly essential for realism and to prevent the flow of conduction current from the case into contacting regions of human tissue, which would otherwise have caused problems due to the use of a grasping hand and a natural orientation of the handset, pressed against the side of the face.

The use of a natural orientation was adopted in the majority of cases, as being consonant with the goal of maximum realism. The result of this was that the monopole antenna was not parallel to any of the principal axes of the FDTD rectangular co-ordinate system. The wire of the antenna is then represented in a 'staircased' form and the length of the conducting surface appears increased by a factor of up to $\sqrt{3}$ (fig. 3). To compensate for this, an algorithm to increase the propagation velocity of waves on the surface of the wire in relation to the degree of staircasing was devised, such that the apparent length of the wire remained constant as it was re-oriented [14]. Other groups have avoided this problem by leaving the antenna and phone in the most convenient orientation and reorienting the head instead. While this has the advantage of simplicity, it avoids the issue of the need to study more complex antenna designs with wire segments that do not lie only parallel to the orthogonal principal axes. It also normally means that the size of the computational domain is increased to accommodate the tilted head.

Fig. 2. Classified head image with uppermost quarter removed.

The near-field and far-field patterns for all orientation angles of the phone were found to be in good agreement when normalized to the same output power [14]. The output power varied by less than 6% over orientation angles from 0 to 45 degrees when using a spatial resolution of 0.0152λ.

2.3 Human Hand Representation

It was believed, from an early stage, that it was important to model the hand grasping the telephone since it must interact significantly with the electromagnetics of the system, as the chassis acts as a counterpoise to the antenna. Within the IBREHT project, a 'block hand' was adopted, which could wrap around a rectangular representation of a telephone body of a size appropriate to the period. The external dimensions of the approximate model hand were obtained by averaging measurements made on a number of human hands. The internal structure of the hand had an internal core of bone, surrounded by a uniform 2.5mm layer of muscle and then a uniform 2.5mm layer of skin. A particular innovation was that the hand incorporated a thumb that pointed upwards and hence could come very close to the antenna. The hand was wrapped around three sides of the model handset with the thumb pressed against one edge. Figure 3 shows the head, handset and hand configuration with the 2.5mm FDTD cell size used in many of the earlier studies.

Fig. 3. Simulation including block hand with thumb. Note 'staircasing' of monopole.

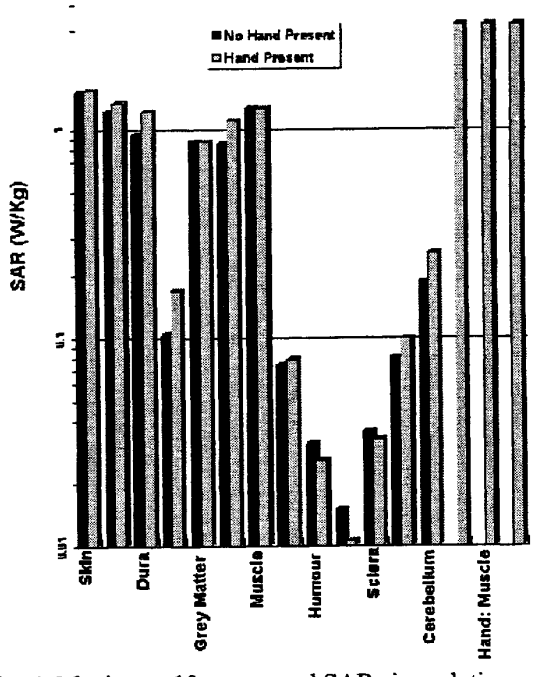

Fig. 4. Maximum 10g-averaged SARs in each tissue type with and without block-shaped hand with thumb (1W radiated from handset at 1.8GHz).

The peak SAR values, averaged over any 10 gram mass were then computed for each tissue of the head and hand. Figure 4 shows the maximum average SAR results obtained in each tissue type with and without the hand. Most immediately apparent are the large SAR values in the tissues of the hand when compared with those in the head: a factor of approximately two times higher than those for the head skin. The location of peak SAR was found to be in the thumb adjacent to the handset, although it may be noted that many standards specify a larger averaging mass for non-head tissue, which would greatly reduce the average SAR.

The SAR levels shown in the head also exhibit an interesting feature when the hand is added: a significant reduction for the tissues located predominantly towards the front of the classified head, in particular the tissues of the eyes. Most other tissues have essentially unchanged, or slightly higher, SAR levels.

2.4 Results

A realistic orientation of the handset was chosen, held at a natural angle (45° to the vertical axis) and rotated transversely to be pressed against the cheek. For this stage of the work, the handset was modeled with a quarter-wavelength monopole antenna, the length being adjusted appropriately for 900 MHz and 1800 MHz. The models were all run twice, with two different FDTD cell resolutions: 2.5mm and 2mm.

The SAR averaging volume was taken as a cube and was centered on the local cell of interest: the volume was chosen to be the nearest number of cells that satisfied the mass criterion (i.e. 1, 10 or 100g). The mass-averaged SAR at tissue surfaces was obtained by letting the cubical volume increase into the surrounding air. The extent to which the resulting value can be said to represent the mass-averaged SAR at surface locations is a matter of ongoing debate. More refined methods for the SAR averaging procedure were developed, in collaboration with other workers, during the CEPHOS project [18].

The total radiated power was found by integrating the Poynting vector around the surface specified as the limit of the FDTD grid, and then adding the power dissipated in cells loaded with lossy material. All computed values of SAR were then divided by this figure, to normalize them to 1W source power. Quantitative values of maximum SAR found at the two frequencies, for different averaging masses, and for the two resolutions, are given in Table 2.

The agreement between the sets of results at 2.5mm and 2mm resolution is reasonably good (15% deviation or less), except for the case of 900MHz with 100g averaging mass: the reason for the discrepancy in this case is not clear. Taken in general, these results serve as an additional validation of the program, as well as giving some indication of the level of uncertainty in the SAR results.

Table 2 Maximum SARs at 900 MHz and 1.8 GHz (The transmitted power was 1W in all cases).

Resolution	Averaging mass	Maximum SARs	
		900 MHz	1.8 GHz
2.5mm	1g	4.2 W/kg	8.2 W/kg
2mm	1g	3.5 W/kg	9.1 W/kg
2.5mm	10g	2.5 W/kg	5.9 W/kg
2mm	10g	2.8 W/kg	5.8 W/kg
2.5mm	100g	1.2 W/kg	2.0 W/kg
2mm	100g	1.6 W/kg	2.2 W/kg

2.5 Parallel Computation Options

The tests quoted above were undertaken with 2.5mm and 2mm resolution, because the numbers of FDTD cells in these cases were approximately one million and two million respectively and these numbers represented the maxima that could be handled by the Unix workstation computers used. As stated above, the desirable target resolution for optimum realism was considered to be 1mm, but this would require about 20 million cells. Until very recent times, the running of problems of this size on serial computers was not practical and hence the use of parallel computers was investigated, experiments in this being run as part of the PEPSE project [2]. The models tested used the realistic head image but no hand: they were principally intended to demonstrate proof of the concept and to investigate the parallelism gains that could be achieved. The speed-up achieved was good [15] but it was not possible to derive definitive values of SAR in the course of the brief runs on distant and costly supercomputers. This mirrors the view in industry that parallel computers are too costly, and work in this area has now shifted to the use of very low-cost 'Beowulf' networks of standard personal computers. Even though the head is now amenable to modeling by state-of-the-art serial computers, parallel techniques will still be necessary for high-resolution models of the whole body, or for simulation of microscopic effects in tissue (e.g. at the cell level).

3. Recent Work (CEPHOS Project)

3.1 Development of PML code

In 1994, a paper by Berenger [16] marked a considerable advance in ABCs. The so-called Berenger perfectly matched layer (PML) was quickly adopted for use in various methods, including the FDTD method [17]. The improvement in this approach was to obtain matching independent of frequency, angle of incidence, and polarization. Berenger proceeded via the application of a field splitting technique to the fields within the PML layer, assigning electric and magnetic conductivities to the fields in the layer such that in theory the medium is perfectly matched to the interior domain, irrespective of

frequency, polarization and angle of incidence. However, implementation in the FDTD method using the Yee staggered grid causes some impedance mismatch at the interior/PML interface resulting in some reflection. The reflection can be minimized by implementing a smooth conductivity profile within the PML, increasing smoothly from small values at the domain/PML interface to larger values at the outer boundary, formed by a PEC/PMC wall.

For the CEPHOS project, commenced in 1997, it was clear that PML had become the ABC of choice and hence a new FDTD program was written which implemented this. The PML that was created uses a geometrical conductivity profile, and has been employed in a wide range of electromagnetic studies involving open boundaries, including those within the CEPHOS project. The values chosen for the parameters of the PML (grading factor, layer thickness, etc) were guided by considerations of possible instability in the solution due to reflection of evanescent waves from the PML [17,18].
Extensive validation tests were undertaken, prior to the computations of SAR in realistic scenarios, involving trials in comparison with the software of four other groups. The main test object was a sphere of brain-like material irradiated by a dipole in close proximity. The results for SAR, averaged over 10g, showed good agreement amongst the participating groups: full results are given in ref. [19].

3.2 Articulated Hand

Numerical dosimetric studies of mobile telecommunications equipment conducted thus far exhibit considerable disparity between the realism adopted for models of the head based on medical imaging scans, and the rather simplistic models used to represent the hand. This may be in large part due to the statements in documents of both the FCC [20] and CENELEC [21] that modeling of the hand is not required for compliance evaluation of handheld mobile telecommunication devices. This guidance is based on some published results that indicate that the presence of the hand tends to reduce the absorbed dose in the head (the region of most interest in such matters). Furthermore, the basic restriction on absorbed dose in the limbs is twice that for the head, although it is not obvious that current devices will not exceed the basic restriction on SAR in the hand (4 W/kg averaged over 10g, per the ICNIRP guide). Others have found [22] that the inclusion of a partially realistic hand can indeed increase the SAR in the head and hence it appears advisable to include it where possible.

The deployment of a more realistic and (more importantly) articulated hand model may also prove to be useful in future studies of handheld MTE, particularly as such devices reduce to sizes comparable to that of the palm of the hand. An anatomically realistic hand model that could be easily articulated to provide a natural-looking posture, and easily integrated into the FDTD software was thus developed [9]. The approach thus far has been based on a simple model, with segments consisting of only bone and muscle. The focus has so far been on the implementation of an articulation scheme by which the posture of the hand can be easily modified.

The hand was divided into its major parts: the palm and the five digits, each digit being further divided into three segments, as shown in Fig. 5. The underlying structure of the hand was provided by nineteen circular cylinders representing the metacarpals and phalanges. These segments form the framework for articulation of the final model, the full description of the hand being provided by the dimensions and relative orientations of these segments. Hemispheres are included at the end of each cylinder to provide greater realism. The bones are covered with muscle in the shape of a rectangular block representing the palm and circular cylinders the fingers and thumb, the end of the digits being finished with hemispheres of muscle.

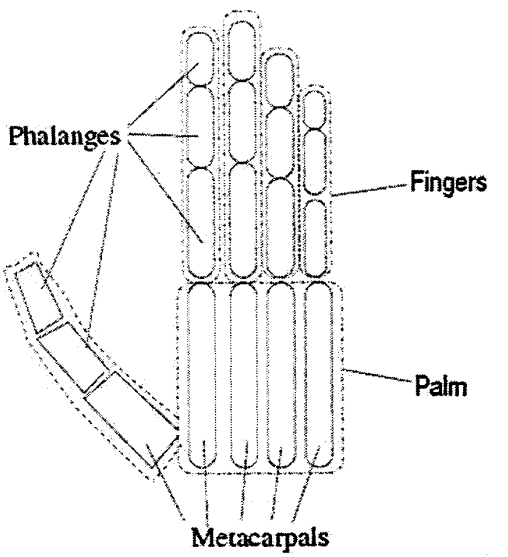

Fig. 5. Basic structure of articulated hand, using regular cylinders with spherical end-caps to simulate the bone, surrounded by a layer of skin (dotted).

The angles shown in Fig. 6a are defined relative to the axis of the previous segment for the second and third phalange and relative to the plane of the palm for the first phalange. The orientation of the palm is defined in relation to an upward-facing (in the positive z-direction) palm lying in the x-y plane as in Fig. 6c, with the fingers aligned parallel to the x-axis.

The construction of each of the 15 segments of the digits of the hand was treated separately. For each cylindrical section representing a segment of a finger the centre of the circular face nearest the palm was established as a

reference point for the construction of that section. For the phalanges joining the metacarpals the reference points are easily determined from the three angles specifying the orientation of the palm. Reference points of the other phalanges require not only the three angles relating to the palm but also the two angles specifying the orientation of the previous phalange of the finger. From a knowledge of the reference point of each segment the hand can be built up by individually constructing the appropriate segment at the relevant location in space.

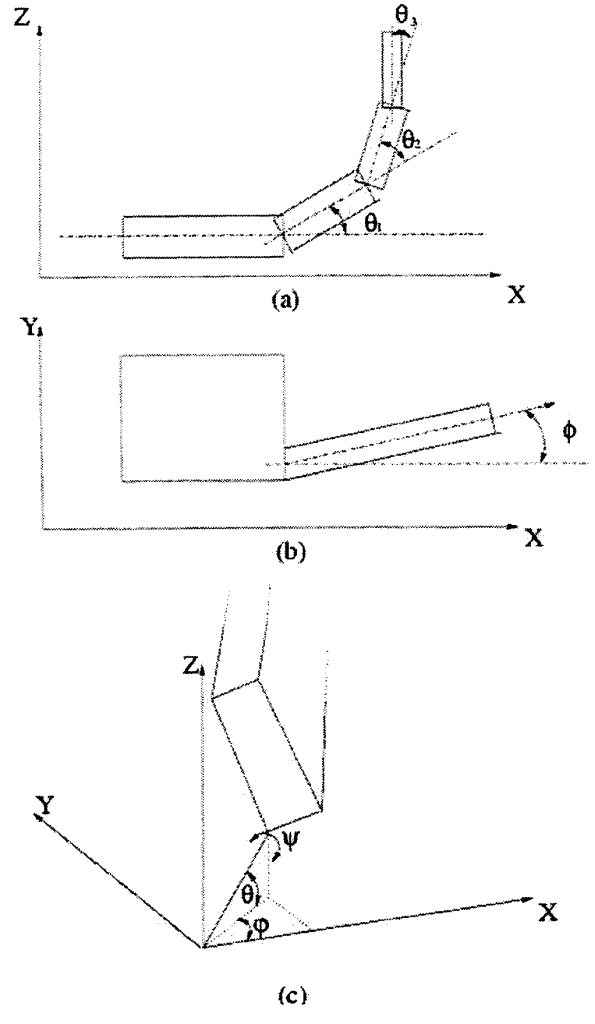

Fig. 6. Details of the angles used to position the hand model. (a) Individual of the three segments of each digit. (b) Rotation of each digit in the plane of the palm. (c) The angles of rotation defined for the hand as a whole.

The transformation for each segment of the hand is implemented as a simple succession of matrix operations, as follows:

$$[x_{old} \quad y_{old} \quad z_{old}]ABCDE = \begin{bmatrix} x_{new} \\ y_{new} \\ z_{new} \end{bmatrix} \qquad (1)$$

Where A implements the positive rotation about the z-axis, B implements the positive rotation about the y-axis, C implements the positive rotation about the x-axis, D implements the rotation ϕ shown in Fig. 6b and E implements the rotation θ shown in Fig. 6a.

For those sections of the hand belonging to the palm, only three rotations are required, corresponding to the angles in Fig. 6c. The (x,y,z) position of a rotated point is then converted into a corresponding cell location in a three-dimensional voxel dataset. The orientation of the thumb was treated using the same rotations as for the fingers, which minimizes complexity at the expense of anatomical accuracy. This was considered a reasonable compromise for a first model. Work is now in progress to replace the artificial components of the hand with realistic ones, taken from the hand of the 'Visible Human' dataset.

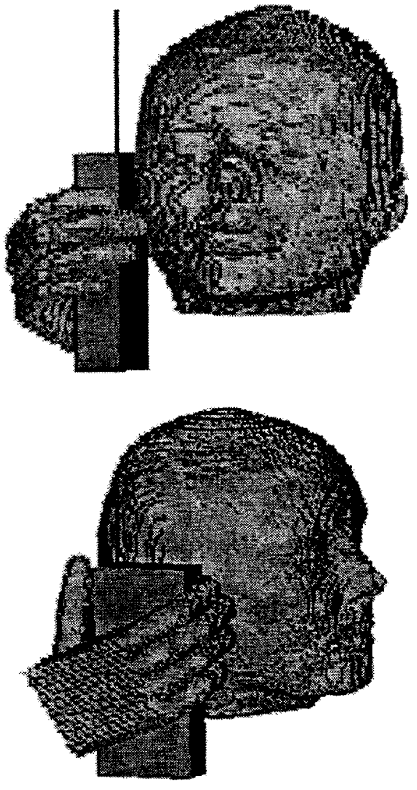

Fig. 7. Head-hand-handset combinations used in CEPHOS studies. (a) 900 MHz model with 2.5mm resolution; (b) 1.8 GHz model with 2mm resolution.

3.3 Results with Head and Hand

The hand model has been used in recent studies involving simulated hand-held telephones and realistic anatomical models of the human head [3]. Fig. 7 shows the hand in use in a Finite-Difference Time-Domain (FDTD) dataset. A generic dielectric-coated handset with an offset quarter-wavelength monopole antenna was used. At this stage of the work it was not feasible to rotate the handset, and

hence it was represented with vertical orientation: rather than building the rotation algorithm into the new program, efforts were concentrated into the hybrid method (see below), which gives fare more flexibility in choice of the orientation of the handset and its components. Illustrative plots of the SAR normalized to a radiated power of 1W at 900 MHz, in axial and coronal slices, are shown in Figs. 8 and 9, respectively. Fig. 10 is similar to Fig. 8, but is for the 1.8 GHz case with 2mm resolution, as shown in Fig. 7b. The numerical results for these two simulations are presented in Table 3.

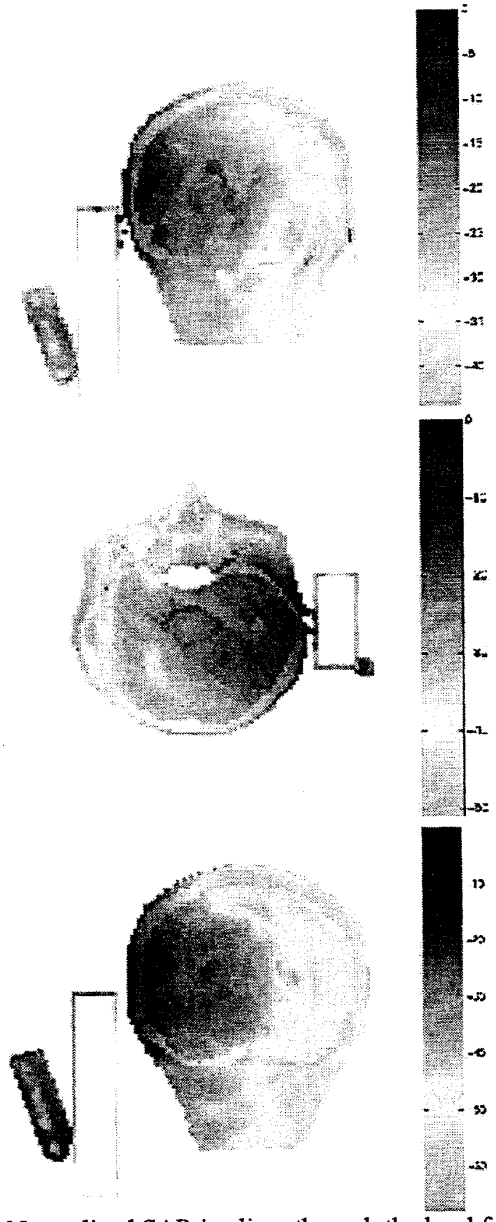

Fig. 8. Normalized SAR in slices through the head for the models in Fig. 7. Scale in dB relative to maximum. Top: coronal slice at 900 MHz, 2.5mm resolution. Centre: axial slice at 900 MHz, 2.5mm resolution. Bottom: coronal slice at 1.8 GHz, 2mm resolution.

Points to be noted in Fig. 8 and Table 3 include:

a. A small amount of loss was incorporated in the dielectric case of the telephone, so that it became visible in the diagrams.

b. Relatively high SAR is visible in the ear and brain adjacent to telephone, as expected, but high values are also noticeable in the tip of the thumb and the palm of the hand, despite looser contact with the telephone than was the case with a 'block' hand.

c. Weak standing waves are visible in the low-SAR region on the side of the head away from the telephone (the effect is more clearly visible in color versions of the images): they are more pronounced at 1.8 GHz than at 900 MHz.

d. At 1.8 GHz there is more concentration of SAR near the surface of the head and higher SAR in the palm of the hand than is the case at 900 MHz.

e. The input impedance of the monopoles is not greatly different from the expected free-space values (i.e. of the order of 40Ω, resistive).

f. A very large proportion of the power is absorbed in the hand at 1.8 GHz (33%). This suggests that neglect of the hand in simulations is inadvisable.

g. The SARs in the head are broadly at the expected levels, although somewhat lower than the values given in Table 2.

h. With 10g averaging, the region of maximum SAR is centered in the brain, as expected. With 1g averaging, it is centered in bone (i.e. skull), which seems surprising. This, however, is an anomaly: the high SARs are in the skin and brain either side of the skull, but the centre of the 1g averaging cube happens to lie in the relatively low-dissipation bone region.

Table 3. FDTD results for a λ/4 monopole on a generic dielectric-coated handset irradiating a realistic model of the head with an articulated model of the hand.

	900 MHz	1.8 GHz
Power radiated (W)	1.0	1.0
Antenna Impedance, Ω	47.2-j1.60	43.78-j7.50
Power absorbed in head, W	0.54	0.36
Power absorbed in the hand, W	0.08	0.33
Max. 1g-average SAR in the head, W/kg	6.53	6.87
Tissue type at centre of max. SAR (1g ave.)	bone	bone
Max. 10g-average SAR in the head, W/kg	4.60	3.41
Tissue type at centre of max. SAR (10g ave.)	white matter	gray matter

3.4 Simulation of Helical Antennas

Over the course of the earlier work, it had become clear that normal-mode helical antennas were at least as popular as monopole types on mobile telephones, and were becoming more popular. Although a square approximation to a helical antenna can be constructed, with care, using the 'staircased' mesh of FDTD, it is rather unsatisfactory and it is almost impossible to angle it to a natural orientation adjacent to the head. Moreover, the helical antenna, if it is to be modeled precisely, must be recognized to be much more complex than merely a coiled filamentary current. The current distribution along its length is obviously non-uniform, but there is also non-uniformity in the surface current distribution around the wire cross-section, and the self-capacitance between the windings causes some current to flow transversely in the wire, especially when the structure is self-resonant. Detailed modeling of the behavior of normal-mode helical antennas had been undertaken previously [23] and this was used to simulate helical antennas on telephone handsets. The work had necessarily used an integral-equation formulation which was not directly compatible with FDTD, and hence a hybrid method was developed to enable a sub-domain to be treated by MoM within the FDTD space. This proved to be highly successful, but it is fully discussed elsewhere and hence will not be repeated in depth here [24-26].

4. Conclusions

It has been argued that realism in the simulation, beyond the level that is sufficient on physical grounds, is essential to convince the non-specialist public of the trustworthiness of computational simulation of SAR in the human body. Initiatives to maximizing this realism have included: use of a tissue-classified three-dimensional magnetic resonance image of human head; the targeting of high resolution in FDTD simulations (down to 1mm); incorporation of representations of a human hand into the model; realistic modeling of mobile telephones, including plastic cases, helical antennas and arbitrary natural orientations; and use of a thermal model for the human head to compute actual temperature rises. This policy of maximizing realism has been proven to be feasible and desirable.

Very high resolutions place heavy demands on computational resources: successful use of parallel computers for this purpose has been demonstrated, but the lower cost option of 'Beowulf' networks now needs to be explored.

In the SAR computations, high values were observed in the tip of the thumb and the palm of the hand, and a very large proportion of the power was absorbed in the hand in some circumstances. This suggests that neglect of the hand in simulations is inadvisable.

The computational modeling process has now reached a high stage of refinement, but the ease of use is still significantly deficient and the incorporation of all of the tools within a suitable graphical user interface is now a very desirable next step.

References

1. EPSRC/DTI 'LINK' Personal Communications Programme final report 'Interaction of the Body with the Radio Emissions from Hand-held Transceivers - IBREHT', Chilton, U.K.: National Radiological Protection Board, 1997.
2. 'Parallel Electromagnetic Programming Support Environment (PEPSE)', Final report to European Union DG XIII, in ESPRIT III project report 'Europort 2', 1996.
3. Final Report to DG XII of EU on Project CEPHOS (Cellular Phones Standard): Electromagnetic Dosimetry for Mobile Communication Equipment, 1999.
4. Vaul, J.A and Excell, P.S.: 'The European CEPHOS (Cellular Phone Standard) Dosimetry Project', IEE Conf. on Antennas and Propagation (Pub. No. 461), York, pp. 65-8, 1999.
5. Coffey, E.L.: 'Recent enhancements to GEMACS 5.2'. Proc. Ninth Annual Review of Progress in Applied Computational Electromagnetics, Monterey, USA, pp. 894-900, 1993.
6. Holland, R.: 'THREDE: A free-field EMP Coupling and Scattering Code'. IEEE Trans. Nuclear Science, Vol. NS-24, pp. 2416-2421, 1977.
7. Mei, K.K., and Fang, J.: 'Superabsorption - a Method to Improve Absorbing Boundary Conditions'. IEEE Trans. Antennas and Propagation, Vol. 40, pp. 1001-1010, 1992.
8. Holland, R., and Simpson, L.: 'Finite Difference Analysis of EMP Coupling to Thin Struts and Wires', IEEE Trans. Electromagnetic Compatibility, Vol. EMC-23, pp. 88-97, 1982.
9. Caputa, K., Okoniewski, M. and Stuchly, M.A.: 'An Algorithm for Computations of the Power Deposition in Human Tissue', IEEE Ant. & Prop. Mag., Vol. 41, No. 4, pp. 102-107, 1999.
10. Joines, W.T. and Spiegel, R.J.: 'Resonance Absorption of Microwaves by the Human Skull', IEEE Trans. Biomed. Eng., Vol. BME-21, pp. 46-49, 1974.
11. Dimbylow, P.J. and Gandhi, O.P.: 'Finite-Difference Time-Domain Calculations of SAR in a Realistic Heterogeneous Model of the Head for Plane-Wave Exposure from 600 MHz to 3GHz', Physics in Med. & Biol., Vol. 36, pp. 1075-1089, 1991.
12. Vaul, J., Excell, P.S. and Olley, P.: 'Numerical Realisation of Realistic Head and Hand Models for Mobile Telephone Safety', Proc. British Computer Society Conf. 'Digital Content Creation', Bradford, Apr. 2000.

13. Luebbers, R., Chen, L., Uno, T., and Adachi, S.: 'FDTD Calculation of Radiation Patterns, Impedance, and Gain for a Monopole Antenna on a Conducting Box'. IEEE Trans. Antennas and Propagation, Vol. 40, pp. 1577-1583, 1992.
14. Excell, P.S., Olley, P. and Jackson, N.N.: 'Modelling of an Arbitrarily-Oriented Mobile Telephone Handset in the Finite-Difference Time-Domain Field Computation Method', ACES J., Vol. 11, No. 2, pp 55-65, 1996.
15. Excell, P.S., Tinniswood, A.D. and Haigh-Hutchinson, K.: 'Parallel Computation of Large-Scale Electromagnetic Field Distributions', ACES J., Vol. 13, No. 2, pp179-187, 1998.
16. Berenger, J.-P.: 'A perfectly matched layer for the absorption of electromagnetic waves,' J. Computat. Phys., pp.185-200, 1994
17. Berenger, J.-P.: 'Perfectly matched layer for the FDTD solution of wave-structure interaction problems,' IEEE Trans. Ant. Prop., pp.110-117 Vol. 44, 1996.
18. Berenger, J.-P.: 'Evanescent Waves in PMLs: Origin of the Numerical Reflection in Wave Structure Interaction Problems', IEEE Trans. Antennas & Prop., Vol. 47, No. 10, pp. 1497-1503, 1999.
19. Nikita, K.S., Cavagnaro, M., Bernardi, P., Uzunoglu, N.K., Pisa, S., Piuzzi, E., Sahalos, J.N., Krikelas, G.I., Vaul, J.A., Excell, P.S., Cerri, G., Chiarandini, S., DeLeo, R. and Russo, P.: 'A Study of Uncertainties in Modeling Antenna Performance and Power Absorption in the Head of a Cellular Phone User', IEEE Trans. Microwave Theory and Techniques, Vol. 48, No. 12, pp. 2676-2685, 2000.
20. FCC OET Bulletin 65 Supplement C, 'Evaluating compliance with FCC guidelines for human exposure to radiofrequency electromagnetic fields,' Federal Communications Commission, Office of Engineering and Technology, 1997.
21. ES 59005 CENELEC, 'Considerations for the evaluation of human exposure to electromagnetic fields (EMFs) from mobile telecommunications equipment in the range 30MHz-6GHz, Comité Européen de Normalisation Electrotechnique, 1998.
22. Watanabe, S.-I., Taki, M., Nojima, T. and Fujiwara, O.: 'Characteristics of the SAR Distributions in a Head Exposed to Electromagnetic Fields radiated by a Hand-Held Portable Radio', IEEE Trans. Microwave Theory & Tech., Vol. 44, No. 10, pp. 1874-1883, 1996.
23. Abd-Alhameed, R.A. and Excell, P.S.: 'Analysis of a Normal-Mode Helical Antenna Including Non-Uniform Wire Surface Current Effects', IEE Proceedings on Microwaves, Antennas and Propagation, Vol. 146, No. 1, pp. 1-5, 1999.
24. Abd-Alhameed, R.A., Excell, P.S., Vaul, J.A. and Mangoud, M.A.: 'A Hybrid Treatment for Electromagnetic Field Computation in Multiple Regions', Electronics Letters, Vol. 34, No. 20, pp 1925-1926, 1998.
25. Mangoud, M.A., Abd-Alhameed, R.A. and Excell, P.S.: 'Simulation of Human Interaction with Mobile Telephones using Hybrid Techniques over Coupled Domains', IEEE Trans. Microwave Theory and Techniques, Vol. 48, No. 11, pp. 2014-2021, 2000.
26. Mangoud, M.A., Abd-Alhameed, R.A. and Excell, P.S.: 'A Heterogeneous Hybrid Computational Electromagnetics Formulation Including Conduction Current Crossing the Domain Boundary', ACES J., present issue.